

Direct spatiotemporal measurements of accelerating ultrashort Bessel-type light bullets

Heli Valtna-Lukner,^{1,*} Pamela Bowlan,² Madis Lõhmus,¹
Peeter Piksarv,¹ Rick Trebino,² and Peeter Saari^{1,*}

¹Institute of Physics, University of Tartu, Riia 142, Tartu, 51014 Estonia

²Georgia Institute of Technology, School of Physics 837 State St NW, Atlanta, GA 30332 USA

* heli.lukner@ut.ee

Abstract: We measure the spatiotemporal field of ultrashort pulses with complex spatiotemporal profiles using the linear-optical, interferometric pulse-measurement technique SEA TADPOLE. Accelerating and decelerating ultrashort, localized, nonspreading Bessel-X wavepackets were generated from a ~ 27 fs duration Ti:Sapphire oscillator pulse using a combination of an axicon and a convex or concave lens. The wavefields are measured with ~ 5 μm spatial and ~ 15 fs temporal resolutions. Our experimental results are in good agreement with theoretical calculations and numerical simulations.

©2009 Optical Society of America

OCIS codes: (320.0320) Ultrafast optics; (320.5540) Pulse shaping;

References and links

1. H. E. Hernández-Figueroa, M. Zamboni-Rached, and E. Recami, eds., *Localized Waves: Theory and Applications* (New Jersey: John Wiley & Sons Ltd, 2008).
2. P. Saari, and K. Reivelt, "Evidence of X-Shaped propagation-invariant localized light waves," *Phys. Rev. Lett.* **79**(21), 4135–4138 (1997).
3. H. Sõnajalg, M. Rätsep, and P. Saari, "Demonstration of the Bessel-X pulse propagating with strong lateral and longitudinal localization in a dispersive medium," *Opt. Lett.* **22**(5), 310–312 (1997).
4. K. Reivelt, and P. Saari, "Experimental demonstration of realizability of optical focus wave modes," *Phys. Rev. E Stat. Nonlin. Soft Matter Phys.* **66**(5), 056611 (2002).
5. I. Alexeev, K. Y. Kim, and H. M. Milchberg, "Measurement of the superluminal group velocity of an ultrashort Bessel beam pulse," *Phys. Rev. Lett.* **88**(7), 073901–073904 (2002).
6. R. Grunwald, V. Kebbel, U. Griebner, U. Neumann, A. Kummrow, M. Rini, E. T. J. Nibbering, M. Piché, G. Rousseau, and M. Fortin, "Generation and characterization of spatially and temporally localized few-cycle optical wave packets," *Phys. Rev. A* **67**(6), 063820–063825 (2003).
7. F. Bonaretti, D. Faccio, M. Clerici, J. Biegert, and P. Di Trapani, "Spatiotemporal amplitude and phase retrieval of Bessel-X pulses using a Hartmann-Shack sensor," *Opt. Express* **17**(12), 9804–9809 (2009).
8. P. Bowlan, H. Valtna-Lukner, M. Lõhmus, P. Piksarv, P. Saari, and R. Trebino, "Measuring the spatiotemporal field of ultrashort Bessel-X pulses," *Opt. Lett.* **34**(15), 2276–2278 (2009).
9. G. A. Siviloglou, J. Broky, A. Dogariu, and D. N. Christodoulides, "Observation of accelerating Airy beams," *Phys. Rev. Lett.* **99**(21), 213901–213904 (2007).
10. P. Saari, "Laterally accelerating airy pulses," *Opt. Express* **16**(14), 10303–10308 (2008).
11. P. Polynkin, M. Kolesik, J. V. Moloney, G. A. Siviloglou, and D. N. Christodoulides, "Curved plasma channel generation using ultraintense Airy beams," *Science* **324**(5924), 229–232 (2009).
12. Z. L. Horváth, and Z. Bor, "Diffraction of short pulses with boundary diffraction wave theory," *Phys. Rev. E Stat. Nonlin. Soft Matter Phys.* **63**(2), 026601–026611 (2001).
13. P. Bowlan, U. Fuchs, R. Trebino, and U. D. Zeitner, "Measuring the spatiotemporal electric field of tightly focused ultrashort pulses with sub-micron spatial resolution," *Opt. Express* **16**(18), 13663–13675 (2008).
14. P. Bowlan, M. Lõhmus, P. Piksarv, H. Valtna-Lukner, P. Saari, and R. Trebino, "Measuring the spatio-temporal field of diffracting ultrashort pulses," *arXiv:0905.4381* (2009).
15. M. Clerici, D. Faccio, A. Lotti, E. Rubino, O. Jedrkiewicz, J. Biegert, and P. Di Trapani, "Finite-energy, accelerating Bessel pulses," *Opt. Express* **16**(24), 19807–19811 (2008).
16. P. Bowlan, P. Gabolde, A. Shreenath, K. McGresham, R. Trebino, and S. Akturk, "Crossed-beam spectral interferometry: a simple, high-spectral-resolution method for completely characterizing complex ultrashort pulses in real time," *Opt. Express* **14**(24), 11892–11900 (2006).
17. P. Bowlan, P. Gabolde, and R. Trebino, "Directly measuring the spatio-temporal electric field of focusing ultrashort pulses," *Opt. Express* **15**(16), 10219–10230 (2007).
18. S. Akturk, B. Zhou, B. Pasquiou, M. Franco, and A. Mysyrowicz, "Intensity distribution around the focal regions of real axicons," *Opt. Commun.* **281**(17), 4240–4244 (2008).

19. D. Abdollahpour, P. Panagiotopoulos, M. Turconi, O. Jedrkiewicz, D. Faccio, P. Di Trapani, A. Couairon, D. Papazoglou, and S. Tzortzakis, "Long spatio-temporally stationary filaments in air using short pulse UV laser Bessel beams," *Opt. Express* **17**(7), 5052–5057 (2009).
 20. J.-M. Manceau, A. Averchi, F. Bonaretti, D. Faccio, P. Di Trapani, A. Couairon, and S. Tzortzakis, "Terahertz pulse emission optimization from tailored femtosecond laser pulse filamentation in air," *Opt. Lett.* **34**(14), 2165–2167 (2009).
-

1. Introduction

Ultrashort, few-cycle optical pulses with special spatiotemporal properties have promising applications in many fields, including physical, quantum, and nonlinear optics; imaging; and particle and cell manipulation; to name a few. These applications often require pulses with a spatial and temporal profile that is much more sophisticated than a simple Gaussian beam in space or pulse in time.

One class of pulses with uncommon, but useful properties are the so-called localized waves [1]. These are ultrabroadband wave packets that are well localized both spatially and temporally and propagate over long distances in linear media without spreading in space or time. Localized waves are difficult to generate experimentally because a specific coupling between the frequency and wavenumber of their Bessel beam constituents is required, and over a broad spectrum. But still several successful experiments have been reported and evidence of the complex spatiotemporal profiles of some types of localized waves has been demonstrated [2–8]. Their distortion-free and superluminal propagation along the cylindrical-symmetry axis has also been observed.

More recently, a type of laterally accelerating localized wave called an Airy beam (or pulse, if generated using ultrashort pulses), has attracted attention [9–11]. Pulses can also accelerate due to diffraction, spherical aberration in lenses, and appropriately shaped nonlinear profiles of axicons [12–15].

In this paper, we report spatiotemporal measurements of accelerating and decelerating Bessel pulses. The term was proposed in [15] where generation and properties of such pulses have been theoretically investigated. These pulses are similar to the localized waves known as Bessel-X pulses [2,3,6–8], with the main difference being that they are generated by crossing and interfering focusing pulses that have curved pulse fronts and form part of a spindle torus surface, rather than the double conical surface that is present in Bessel-X pulses. As a result, their bullet-like, central, intense apex and accompanying Bessel rings become smaller or larger as the pulse propagates, depending on whether the torus shrinks towards a ring or expands towards a sphere. But the central spot of these pulses is still localized and intense over a propagation distance considerably longer than that of a Gaussian beam with a comparable waist size.

To make these measurements we used scanning SEA TADPOLE (Spatially Encoded Arrangement for Temporal Analysis by Dispersing a Pair of Light E-fields) [13,16], which is a linear-optical interferometric method for measuring the spatiotemporal field $E(x,y,z,t)$ of complicated ultrashort pulses. Briefly, this method involves sampling a small spatial region of the Bessel pulse with a single-mode optical fiber and then interfering this pulse with a reference pulse in a spectrometer to reconstruct $E(\lambda)$ for that spatial point. Then to measure the spatial dependence of the field, we scan the fiber axially (in x) throughout the cross section of the Bessel pulse, so that $E(\lambda)$ is measured at each x , yielding $E(\lambda,x)$. This field can be Fourier transformed to the time domain to yield $E(t,x)$. In order to measure the z (propagation direction) dependence of the spatiotemporal field, the axicon and lens are translated along the propagation direction to bring them nearer or further from the sampling point (the fiber). As demonstrated previously [8,13,14,16,17], SEA TADPOLE can measure optical pulses with complex spatiotemporal intensities and phases with sub-micron spatial and femtosecond temporal resolutions.

2. Theoretical description of accelerating Bessel pulses

The formation of accelerating Bessel pulses can be intuitively described using the Huygens-Fresnel principle. This involves treating each point on the wave-front as a source of

spherically expanding waves whose temporal profile is governed by that of the primary wave. Consider an ultrashort pulse impinging on a thin annular slit ($\sim 1 \mu\text{m}$ wide) at an instant $t = 0$. Thinking in terms of the Huygens-Fresnel principle, this will yield an expanding, semi-toroidal wave-field immediately behind the slit. As the pulse propagates further, the tube radius of the half torus becomes larger than the annular-slit radius R , and at times $t > R/c$ the wave-field evolves like a spindle torus, i.e., different parts of the torus start to overlap. Of course, the wave-field is treatable as a mathematical surface only for infinitesimally short delta-like pulses in time. Real ultrashort pulses are at least several cycles long, and so yield an interference pattern in the overlap region (see insets of Fig. 1). The radial dependence of the field in the interference region is approximately a zeroth-order Bessel function of the first kind.

As the wave-field evolves in time, the intersection region propagates along the z -axis and the angle between the normal of the torus surface and the z -axis (θ) decreases. For ultrashort pulses, this intersection region is small, and the angle θ is approximately the same for all points within it at a given instant. Therefore the field in the intersection region is approximately equivalent to the center of a Bessel beam or the apex of a Bessel-X pulse (see also [12]). The smaller the angle θ —also called the *axicon angle*—the larger the spacing between the Bessel rings and the smaller the superluminal velocity of the pulse. Hence, an annular ring transforms an ultrashort pulse into a decelerating Bessel wave-packet propagating along the z -axis. Of course, outside of the intersection region, where there is no interference to generate phase fronts that are perpendicular to the z -axis or a Bessel profile, the phase and pulse fronts expand with a constant velocity c and propagate in their normal directions.

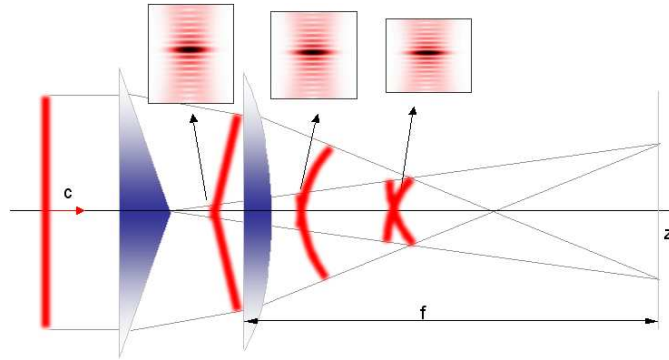


Fig. 1. Schematic of the formation of accelerating pulses from a plane-wave pulse moving to the right with velocity c . The red strips depict the pulses' intensity profiles in space at four different times. The conical surface of the axicon transforms the plane-wave pulse into a Bessel-X pulse, and the convex lens then yields the accelerating pulse. (In the actual experiments, the positions of the axicon and lens were interchanged, but this does not influence the results.) The inset plots show the expected intensity vs. x and t for three different positions z .

Since very little energy passes through an annular slit, it is more efficient to use an axicon in combination with a lens to generate such fields. If the lens is concave, the field behind it evolves similarly to what was described above, and a decelerating pulse is generated. On the other hand, a convex lens (see Fig. 1) results in an increasing angle θ as the pulse propagates and hence an accelerating pulse.

There are two approaches for calculations elaborating the above qualitative treatment. The first approach involves considering only the intersection region close to the optical axis. Here the field is approximately conical, or it is a cylindrically symmetrical superposition of plane waves propagating at a fixed angle θ to the z axis. In this case, the field can be described using the known expression for the field of a Bessel-X pulse, which is a broadband wave-packet of monochromatic Bessel beams [1–3,5–7,15]

$$\Psi(\rho, z, t) = \int_0^{\infty} d\omega G(\omega - \omega_0) J_0 \left[\frac{\omega}{c} \rho \sin \theta(z) \right] \exp \left\{ i \frac{\omega}{c} [z \cos \theta(z) - ct] \right\}, \quad (1)$$

where ρ , z , and t are the spatial (cylindrical) and temporal coordinates, and $G(\omega - \omega_0)$ is the (Gaussian-like) spectrum of the pulse having a central frequency ω_0 . However, unlike the case of the Bessel-X pulse, here the axicon angle depends on the propagation distance z from the lens with the focal length f as $\theta(z) = \arctan[|f(f-z)^{-1}| \tan \theta_a]$, where θ_a is the axicon angle without the lens. Because the group velocity of the wave-packet along the z direction is given by $v_g = c/\cos(\theta)$ [1–3,5–7,15], the group velocity of the Bessel pulses will be superluminal and accelerate if f is positive and decelerate if f is negative. The approximations made in this approach are valid as long as the pulse duration τ is much shorter than its characteristic time of flight given by f/c . Considering our experimental parameters, which are given below, the phase fronts at the intersection (apex) region deviate from those of conical waves by less than 10^{-5} of the wavelength, which is negligible.

The second more general approach involves recognizing that a lens is a Fourier transformer and that the Fourier transform of the field just after the axicon is a good approximation to a thin ring. Therefore the temporally reversed field of the accelerating Bessel pulse can be calculated by integrating over monochromatic spherical wave pulses as if they were emerging from a thin annular slit:

$$\Psi_{sph}(\rho, z, t) \propto \int_0^{\infty} d\omega \int_0^{2\pi} d\varphi r_a \omega G(\omega - \omega_0) \frac{\exp \left\{ i \frac{\omega}{c} \left[\sqrt{\rho^2 + r_a^2 - 2r_a \rho \cos \varphi + z^2} - ct \right] \right\}}{\sqrt{\rho^2 + r_a^2 - 2r_a \rho \cos \varphi + z^2}}. \quad (2)$$

Here $r_a = |f \tan(\theta_a)|$ is the radius of the ring along which the integration is carried out by the polar coordinate φ of the source points and the origin of the z axis is in the plane of the ring. One advantage to this approach is that we can take into account aberrations in the lens and axicon. For example, chromatic aberrations can be modeled using a frequency-dependent ring radius $r_a(\omega)$. Also, this expression can be used for numerical calculations of the field under the conditions in which the previous approach is not valid, i.e., also outside of the apex region.

3. Experimental results

In our experiments, ultrashort, accelerating Bessel pulses were generated using a KM Labs Ti:Sa oscillator with 33 nm of bandwidth (FWHM) and an approximately Gaussian spectrum with a central wavelength $\lambda_0 = 805$ nm. The spot size of the laser beam was 4 mm (FWHM). A fused-silica axicon with an apex angle of 176° was used, which transforms plane wave pulses at $\lambda_0 = 805$ nm into conical wave pulses (Bessel-X pulses) with $\theta_a = 0.92^\circ$. We used lenses with focal lengths of +153 mm and –152 mm. For convenience in the actual set-up, the axicon was mounted behind the lens in a lens tube, i.e., in reverse order of Fig. 1. So the two components effectively constituted a single thin phase element, whose transmission function does not depend on the ordering of components. However, the small distance between them (a few mm) was taken into account in our simulations.

The spatiotemporal field after the compound optic was measured using SEA TADPOLE, using a reference pulse directly from our oscillator. At each position of the sampling fiber in SEA TADPOLE, we measured the spectral phase difference between the reference pulse and the Bessel pulse and its spectrum, so that our measurements reflect the phase added to the beam by the lens and axicon. Such differential measurements also allowed us to add glass to the reference arm of SEA TADPOLE, so that chirp introduced by the axicon and lens would essentially cancel out in the measurement.

Our device had a spatial resolution of about 5 μm , determined by the mode size of the fiber that we use to sample the Bessel pulse. Our temporal resolution was ~17 fs and with zero-filling we reduced the point spacing on the time axis to 4.5 fs. Because the temporal resolution of SEA TADPOLE is given by the inverse of the spectral range of the unknown

pulse, and the smallest possible temporal feature in the pulse is given by the inverse of its bandwidth (which is several times less than the spectral range), our device should always have sufficient temporal resolution to measure the unknown pulse, regardless of its duration (even for single cycle pulses). Because the Bessel pulses were approximately cylindrically symmetrical, we only measured the field along one transverse coordinate, x . For more details about the SEA TADPOLE device that we used, see reference [13].

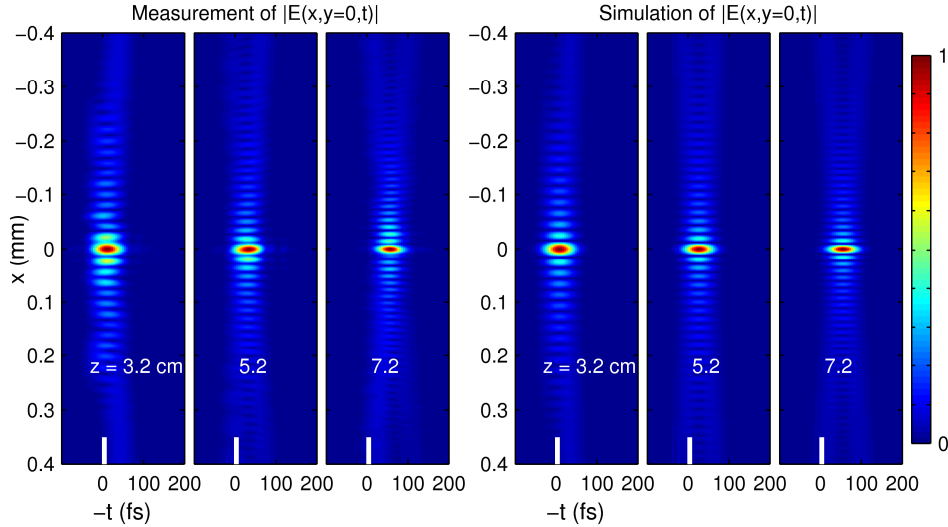


Fig. 2. Comparison of the measured and calculated spatiotemporal profiles of the electric field amplitude of an *accelerating* Bessel pulse at three positions along the propagation axis (z). The color bar indicates the amplitude scale normalized separately for each plot. The white bar emphasizes $t = 0$, which is where the pulse would be located if it were propagating at c .

The spatiotemporal profiles of the accelerating Bessel pulses were measured at five different z positions and for the decelerating Bessel pulse at nine positions. In all cases, we measured the complete spatiotemporal intensity and phase, but we show only the spatiotemporal intensities here, as this information is more interesting. Three of these measurements for each are shown in Fig. 2 and Fig. 4. For comparison, numerical simulations were performed using Eq. (1) with the experimental parameters, and as seen in the figures, the two are in very good agreement.

SEA TADPOLE also measures the Bessel-X pulse's arrival time with respect to the reference pulse, the latter of which, after passing through the compensating piece of glass, travels at the speed of light c . The origin of our time axis can be considered as the location of the reference pulse if it propagated along the axis z with the Bessel pulses. So, if the Bessel pulse were traveling at the speed of light, then, for each value of z , its spatiotemporal intensity would be centered at the same time origin $t = 0$ which is emphasized with the white bar in the figures. But it is easy to see in Figs. 2 and 3 that this is not the case. The superluminal group velocity and the pulse's acceleration or deceleration are both apparent from the z -dependent shifts of the pulses relative the origin $t = 0$. The time shifts were compared to theoretically calculated shift function and we found a good agreement, see Fig. 4.

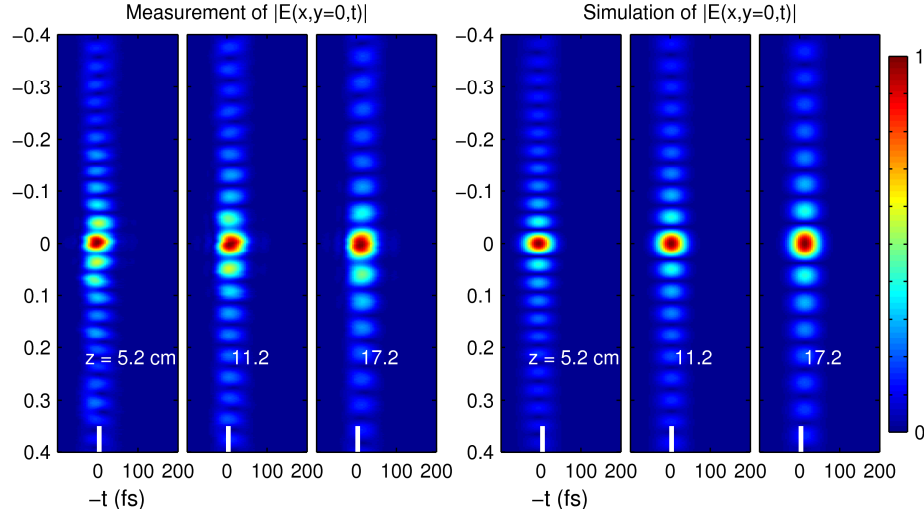


Fig. 3. Comparison of measured and calculated spatiotemporal profiles of the electric field amplitude of *decelerating* Bessel pulse at three positions along the propagation axis z .

The group velocity of Bessel pulses can also—indirectly but in the given case more precisely—be determined from the measured fringes in their spatial profile. This is because these fringes correspond to rings of intensity maxima, radii of which grow sequentially as governed by placement of maxima and minima of the Bessel function J_0 . Thanks to the many measurable fringes we could accurately determine the mean radial wavelength $\Lambda_B = \lambda_0 / \sin\theta$ of the Bessel profile.

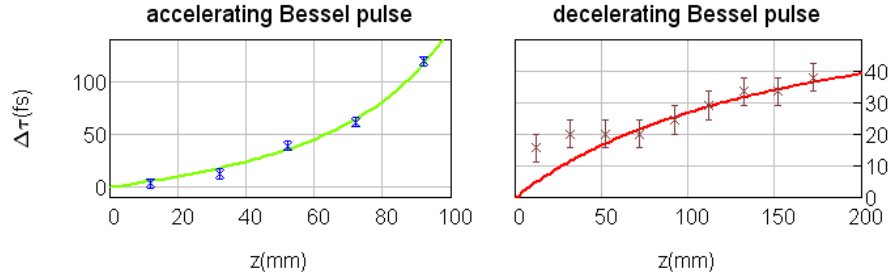


Fig. 4. Experimentally determined (points) and theoretically predicted (solid curves) temporal shifts (in femtoseconds) of the accelerating/decelerating Bessel pulses in respect of the reference pulse. z is the propagation distance.

Hence, having in mind the approximations that apply to Eq. (1) and the relation $v_g = c/\cos\theta$, the distance-dependent group velocity can be found using the following equation:

$$v_g(z) = c / \sqrt{1 - [\lambda_0 / \Lambda_B(z)]^2}. \quad (3)$$

Equation (3) was used to estimate the group velocity of the measured pulses at various propagation distances, and these results are shown in Fig. 5 along with the theoretical values. The experimental values are in good agreement with our theoretical predictions, except for two points at $z = 32$ mm and 52 mm for the decelerating pulses. This discrepancy is likely due to the imperfect surface of the axicon as discussed below.

Without a lens, the propagation depth over which the Bessel-X pulses last, starts, in principle, at the tip of axicon and ends at $z \approx w/\tan\theta_a$, where w is the radius of the input beam or aperture. Imperfections in our axicon reduce the distance over which the Bessel-X pulse maintains its perfect ring profile (let us call it the Bessel zone). At values of z less than 50

mm, the profile distortions were caused by the slightly spherical tip of the axicon (see, e. g., [18]). This axicon aberration also makes the pulse accelerate even without a lens, though this effect is small and did not significantly influence our measurements. Slight deviations of the surface of the axicon from an ideal cone are responsible for a reduction of the upper limit of the zone, which for our axicon stopped at $z \approx 130$ mm [8]. Therefore the Bessel zone only lasted half as long as it would be expected to in the absence of aberrations ($z_{\max} \approx w/\tan\theta_a$). At values of $z > 130$ mm, these deviations distort the phase-fronts of the interfering plane wave constituents of the conical wave to an extent that affects the shape of the central spot of the Bessel profile, but it does not noticeably affect the pulse's group velocity as established in [8] from direct temporal data.

Placing lenses before the axicon compresses or stretches the Bessel zone (see, e. g., [19,20]). Without the lens the Bessel zone for the axicon that we used lasts for 80 mm (= 130 mm – 50 mm). When the positive lens is added, this decreases to about 50 mm, going from $z \approx 30$ mm to 80 mm. With the negative lens (decelerating Bessel pulses) the Bessel zone is greatly lengthened, and in principle to tens of kilometers starting at $z \approx 70$ mm. Therefore the two points at $z = 32$ mm and 52 mm in Fig. 5 deviate (as clearly seen in the right plot with expanded ordinate scale) from the theoretical curve because they are outside of the Bessel zone. Although we could not measure the decelerating pulse kilometers from the axicon, the Bessel ring pattern was observable by eye on the lab wall ~10 m after the axicon, and, at this point, the radial wavelength Λ_B had increased to about 1 mm.

The full width of the central maximum of the accelerating Bessel pulse at $1/e$ of the maximum decreased by a factor of 1.6, from 23.0 μm to 14.8 μm , after 40 mm of propagation from $z = 32$ mm to 72 mm inside the Bessel zone. For the decelerating pulse, the spot size instead increased by a factor of 1.4, from 39.1 μm to 56.0 μm after 10 cm of propagation from $z = 72$ mm to 172 mm. This represents a much larger Rayleigh range than that of a Gaussian beam, which would only be 0.2 mm if the waist diameter were 14.8 μm or 1.5 mm if it were 39.1 μm .

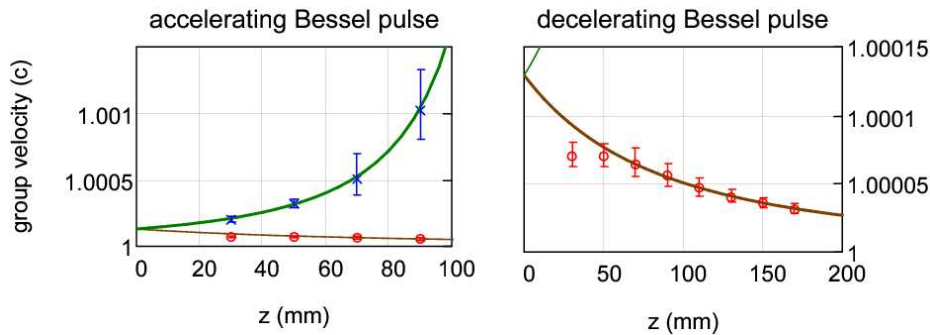


Fig. 5. Comparison of experimentally and theoretically calculated group velocities for accelerating and decelerating Bessel pulses. The measured group velocities for the accelerating Bessel pulses are marked with blue crosses, and, for decelerating pulses, with red circles. The error bars show the standard deviations from the mean value. The solid lines show the theoretically predicted dependences. At the position $z = 0$, the theoretical curves for both pulses coincide because the same axicon was used to generate them.

It should be stressed that the indirect evaluation of the group velocities from the interference patterns is slightly more precise than using the time shift data thanks to relatively high quality of our axicon (except the tip) and relatively narrow spectrum of the input pulse. In the case of shorter pulses—in certain sense “genuine” Bessel-X pulses contain only a few cycles—the number of fringes (Bessel rings) is correspondingly small and their spacing should be measurable with lower accuracy than the time shifts in the plots with femtosecond-range temporal resolution. Similarly, if there are substantial phase distortions present in the optical elements the fringe patterns acquire irregularities; hence again the direct approach based on the time shifts is preferable not only principally but also practically.

5. Conclusions

We directly measured the spatiotemporal field $E(x,t,z)$ of ultrashort accelerating and decelerating Bessel pulses with micron spatial resolution and femtosecond temporal resolution using SEA TADPOLE. The field after a lens and axicon was described and modeled theoretically, and we used this model to analyze our experimental results. The features in the measured spatiotemporal profiles, including the ring spacings and the central spot sizes, were found to be in good agreement with our theoretical calculations and numerical simulations. We also measured the group velocities of the pulses along the propagation direction and observed their acceleration and deceleration. The accelerating Bessel pulse's speed went from $1.0002 c$ after 3.2 cm of propagation to $1.0009 c$ at 7.2 cm and the decelerating Bessel pulse had a speed of $1.00007 c$ after 5.2 cm and $1.00003 c$ after 17.2 cm of propagation. The measured group velocities were also in good agreement with our theoretical calculations.

Acknowledgements

R. Trebino acknowledges support of the Georgia Research Alliance, and P. Bowlan was supported by an NSF fellowship IGERT-0221600 and NSF SBIR grant #053-9595. The Estonian authors were supported by the Estonian Science Foundation, grant #7870.